Dislocated spots and triple splittings of natural rainbows generated by large drop distortions, oscillations and tilts

Supporting information

Alexander Haußmann, April 30th, 2020

1. Raindrop oscillations in a natural rainbow display

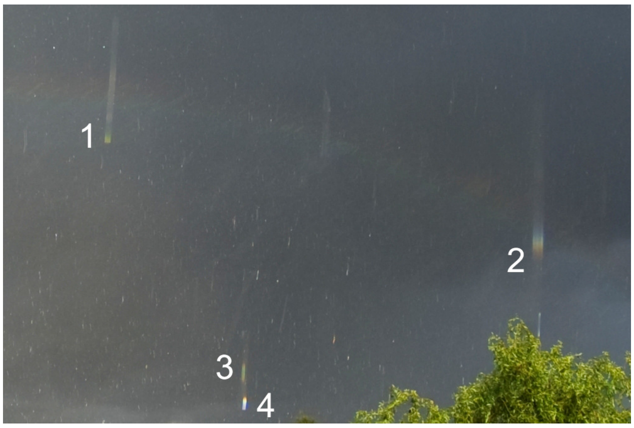

Dresden, Sept. 9th, 2017, 16:13 CEST, left: original photograph, right: cropped section showing four rainbow oscillation streaks from large drops, strongly shifted from the ordinary rainbow position (and some with inverted color ordering)

2. Mathematical details of including the BC shapes into the GO model

for the older 2HS version, see

https://www.meteoros.de/download/haussmann/AHaussmann_SI_JQSRT2016_corrected_161012.pdf

2.1 BC deformation coefficient interpolation

$$c_n = 10^{-4} \cdot \left(B_{2,n} \cdot \alpha^2 + B_{3,n} \cdot \alpha^3 + B_{4,n} \cdot \alpha^4 + B_{5,n} \cdot \alpha^5 \right) \qquad \text{with} \qquad \alpha = \frac{a_0}{1\,\text{mm}}$$

Interpolation coefficients, valid in the size range of $\alpha = 0$ to $\alpha = 2$:

n	0	1	2	3	4	5	6	7	8	9	10
$B_{2,n}$	-58.46	-125.3	-182	-37.69	-7.269	-4.244	-3.137	-2.054	3.143	3.845	4.89
$B_{3,n}$	-153.3	5.208	-448.3	-163.9	-33.77	25.23	18.56	8.366	-9.638	-9.745	-10.26
$B_{4,n}$	94.28	-4.551	301.7	126.7	48.29	-2.639	-10.93	-9.133	4.554	6.265	8.273
$B_{5,n}$	-16.55	5.416	-55.5	-25.31	-11.95	-1.365	1.686	1.951	-0.762	-1.114	-1.869

2.2 Direction of the surface normal

Points on the drop surface in Cartesian coordinates are given by the usual conversion formula for spherical coordinates, including the azimuthal angle φ:

$$\vec{r}(\vartheta,\varphi) = \begin{pmatrix} x \\ y \\ z \end{pmatrix} = r(\vartheta,\varphi) \cdot \begin{pmatrix} \cos\varphi \cdot \sin\vartheta \\ \sin\varphi \cdot \sin\vartheta \\ \cos\vartheta \end{pmatrix}$$

For the equilibrium shapes, $r(\vartheta,\varphi)$ is to be substituted with $r_0(\vartheta)$. For $(l,0)$ modes, $r(\vartheta,\varphi) = r(\vartheta)$ (no φ dependence).

The outward-oriented drop surface normal unit vector $\vec{n}_{out}$, needed in vectorial raytracing for the laws of reflection and refraction, at a point on the drop surface defined by ϑ and φ, can be calculated as follows:

$$\vec{N}_{out} = \frac{\partial \vec{r}}{\partial \vartheta} \times \frac{\partial \vec{r}}{\partial \varphi} = r \cdot \left(r \cdot \sin\vartheta \cdot \vec{e}_r - \frac{\partial r}{\partial \vartheta} \cdot \sin\vartheta \cdot \vec{e}_\vartheta - \frac{\partial r}{\partial \varphi} \cdot \vec{e}_\varphi \right)$$

$$\vec{n}_{out} = \frac{\vec{N}_{out}}{\left|\vec{N}_{out}\right|}$$

$\vec{e}_r$, $\vec{e}_\vartheta$, $\vec{e}_\varphi$ are the conventional unit vectors in spherical coordinates.

Also, in contrast to the 2HS and 3PS models, the size of the target disc encircling the projected drop cross section must be estimated properly before raytracing, in order to encompass all relevant surface points while not including too much empty area around the drop at which the ray candidate will miss the surface. This has also to be done for the extremal oscillation states, and, in case of polydisperse amplitudes, for a suitable upper amplitude limit (e.g. expected value + 3σ).

2.3 List of normalized, real-valued spherical harmonics for l = 2 and l = 3

$$Y_{2,0}(\vartheta,\varphi)=\frac{1}{4}\sqrt{\frac{5}{\pi}}\cdot\left(3\cos^2\vartheta-1\right)$$

$$Y_{2,1}(\vartheta,\varphi)=\frac{1}{2}\sqrt{\frac{15}{\pi}}\cdot\cos\vartheta\sin\vartheta\cdot\cos\varphi$$

$$Y_{2,-1}(\vartheta,\varphi)=\frac{1}{2}\sqrt{\frac{15}{\pi}}\cdot\cos\vartheta\sin\vartheta\cdot\sin\varphi$$

$$Y_{2,2}(\vartheta,\varphi)=\frac{1}{4}\sqrt{\frac{15}{\pi}}\cdot\sin^2\vartheta\cdot\cos 2\varphi$$

$$Y_{2,-2}(\vartheta,\varphi)=\frac{1}{4}\sqrt{\frac{15}{\pi}}\cdot\sin^2\vartheta\cdot\sin 2\varphi$$

$$Y_{3,0}(\vartheta,\varphi)=\frac{1}{4}\sqrt{\frac{7}{\pi}}\cdot\left(5\cos^3\vartheta-3\cos\vartheta\right)$$

$$Y_{3,1}(\vartheta,\varphi)=\frac{1}{8}\sqrt{\frac{42}{\pi}}\cdot\left(5\cos^2\vartheta-1\right)\sin\vartheta\cdot\cos\varphi$$

$$Y_{3,-1}(\vartheta,\varphi)=\frac{1}{8}\sqrt{\frac{42}{\pi}}\cdot\left(5\cos^2\vartheta-1\right)\sin\vartheta\cdot\sin\varphi$$

$$Y_{3,2}(\vartheta,\varphi)=\frac{1}{4}\sqrt{\frac{105}{\pi}}\cdot\cos\vartheta\sin^2\vartheta\cdot\cos 2\varphi$$

$$Y_{3,-2}(\vartheta,\varphi)=\frac{1}{4}\sqrt{\frac{105}{\pi}}\cdot\cos\vartheta\sin^2\vartheta\cdot\sin 2\varphi$$

$$Y_{3,3}(\vartheta,\varphi)=\frac{1}{8}\sqrt{\frac{70}{\pi}}\cdot\sin^3\vartheta\cdot\cos 3\varphi$$

$$Y_{3,-3}(\vartheta,\varphi)=\frac{1}{8}\sqrt{\frac{70}{\pi}}\cdot\sin^3\vartheta\cdot\sin 3\varphi$$

For these and all other normalized real-valued spherical harmonics the orthonormalization condition holds:

$$\int_{\textit{full sphere}} d\Omega\cdot Y_{l,m}(\vartheta,\varphi)\cdot Y_{l',m'}(\vartheta,\varphi)=\delta_{l,l'}\cdot\delta_{m,m'}$$

Reference: D. Pinchon and P.E. Hoggan, “Rotation matrices for real spherical harmonics: general rotations of atomic orbitals in space-fixed axes,” Journal of Physics A: Mathematical and Theoretical **40**, 1597-1610 (2007).

2.4 Relation between axis ratio ξ and (2,0) oscillation elongation $A^*_{2,0} \cdot q$

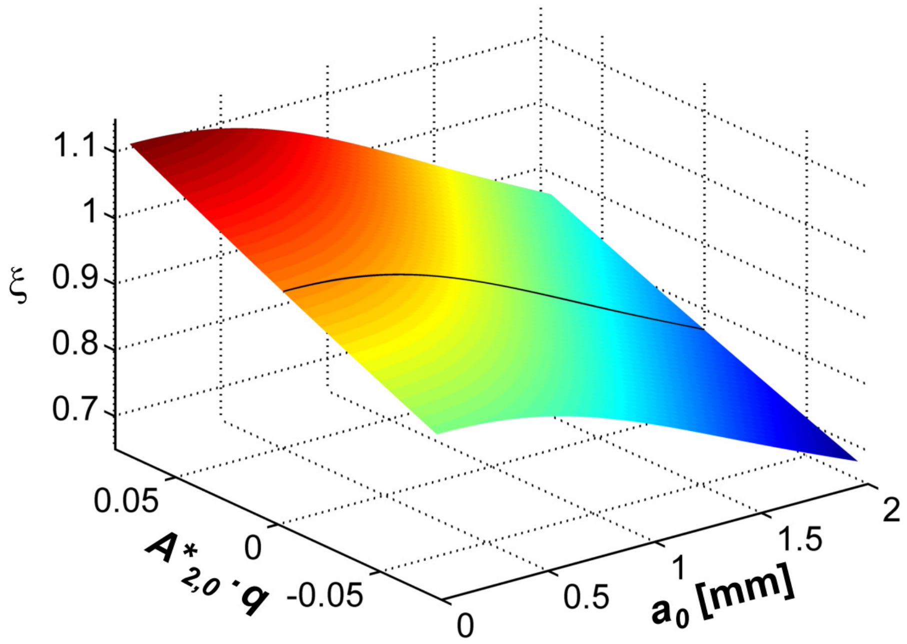

black line = formula for $\bar{\xi}$ from [9], corresponding to zero elongation

2.5 Coordinate transformations for tilted drop axes

transformation from "laboratory" (field) into drop coordinates:

$$\begin{pmatrix} x_D \\ y_D \\ z_D \end{pmatrix} = \underline{M}_{L \to D} \cdot \begin{pmatrix} x_{Lab} \\ y_{Lab} \\ z_{Lab} \end{pmatrix}$$

$$\underline{M}_{L \to D} = \begin{pmatrix} \cos\vartheta_D \cos\varphi_D & \cos\vartheta_D \sin\varphi_D & -\sin\vartheta_D \\ -\sin\varphi_D & \cos\varphi_D & 0 \\ \sin\vartheta_D \cos\varphi_D & \sin\vartheta_D \sin\varphi_D & \cos\vartheta_D \end{pmatrix}$$

ϑ_D, φ_D: axis tilt and tilt azimuth

This matrix is orthogonal, i.e. the inverse is simply the transposed matrix.

For non-axisymmetric oscillations, a third angle ζ_D is required to describe the rotation of the drop itself around a chosen (now non-symmetry) axis, thus completing the set of three Euler angles:

$$\underline{M}_{L\to D} = \begin{pmatrix} \cos\varsigma_D \cos\vartheta_D \cos\varphi_D - \sin\varsigma_D \sin\varphi_D & \cos\zeta_D \cos\vartheta_D \sin\varphi_D + \sin\varsigma_D \cos\varphi_D & -\cos\varsigma_D \sin\vartheta_D \\ -\sin\varsigma_D \cos\vartheta_D \cos\varphi_D - \cos\varsigma_D \sin\varphi_D & -\sin\varsigma_D \cos\vartheta_D \sin\varphi_D + \cos\varsigma_D \cos\varphi_D & \sin\varsigma_D \sin\vartheta_D \\ \sin\vartheta_D \cos\varphi_D & \sin\vartheta_D \sin\varphi_D & \cos\vartheta_D \end{pmatrix}$$

This matrix is also orthogonal.

3. Comparison of Möbius shifts for 2HS and BC model drops calculated by raytracing

- calculated for $a_0 = 0.5$ mm, $n = 1.335$, $A^*_{2,0} = 0.01$, vertical drop axes
- only clock angles for one half arc between 0° (rainbow top) and 180° (rainbow bottom) shown, other half is identical
- small sector between dashed lines: relevant parameter combinations for positive sun elevations and the arc segment above the horizon (= visible part for ground based observer)
- color scaling (white = zero):

<u>primary rainbow</u>

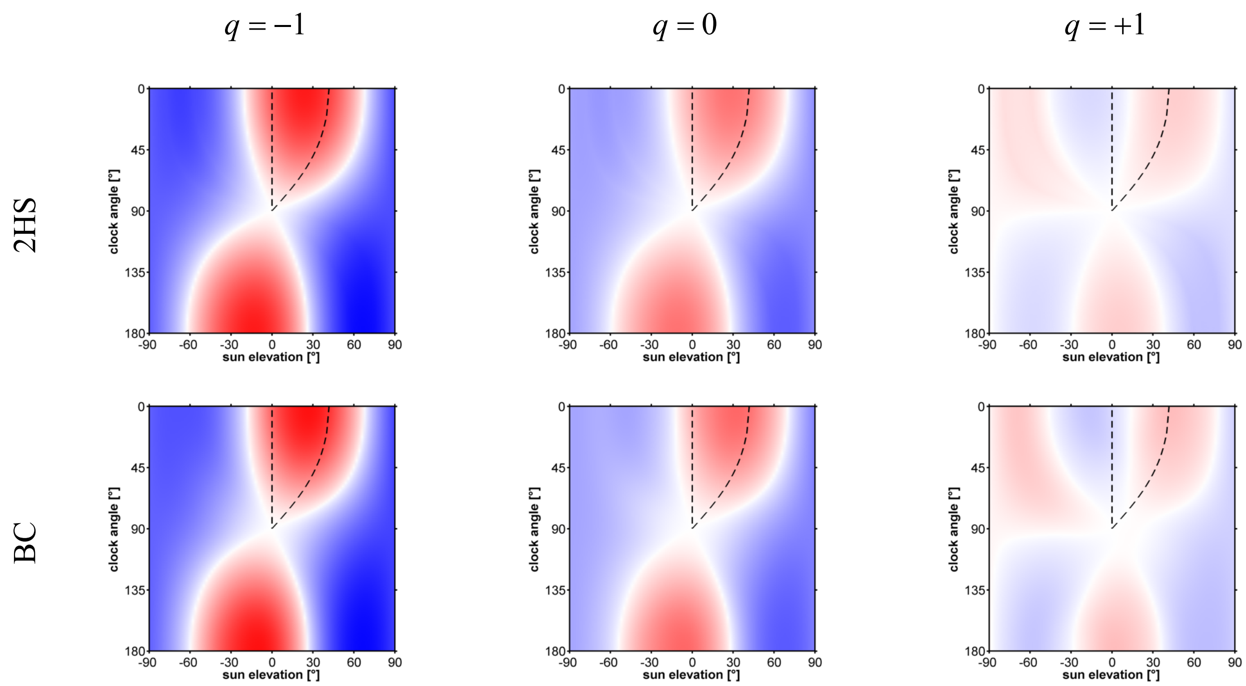

secondary rainbow

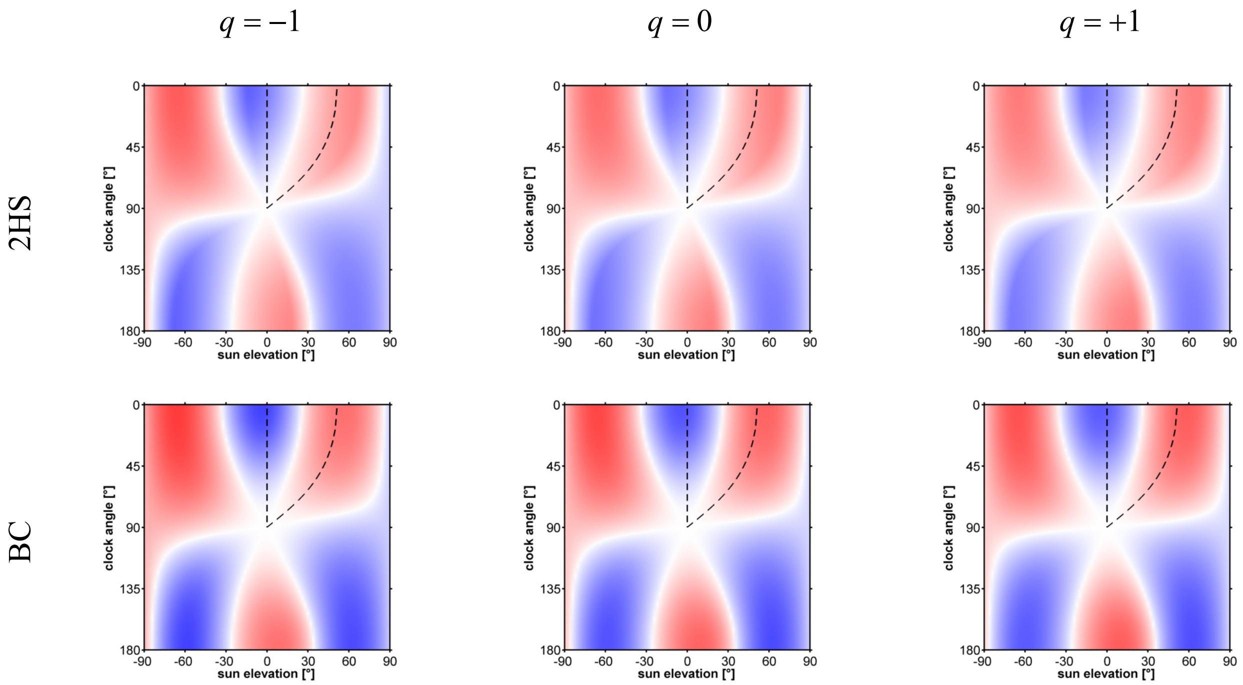

- accuracy of 2HS results acceptable, also for $(2,0)$ oscillations (2HS is faster to calculate, and full simulations require data for all relevant drop sizes, not only $a_0 = 0.5$ mm)
- extremal values of Möbius shifts for the secondary are comparable to those for the primary for $a_0 = 0.5$ mm : often-reported overall near-zero shifts for the secondary are only present in up-down symmetric drop models (1S, but not 2HS or BC)
- (2,0) oscillation is symmetric: secondary's Möbius shift is therefore almost independent on elongation q $\rightarrow$ stability of the secondary against blurring or splitting caused by this oscillation mode
- Möbius shift for the secondary has a zero line through the visibility sector ($h_S = 0°...20°$): main reason for the observed stability of its super-horizon arc against splitting caused by equilibrium drop distortions (and proper eDSDs) [10]
- also, the secondary is broader and thus the shift needs to be larger for a noticeable split

4. Bright spots of the 4th order, and from reversed ray paths of the 2nd and 6th order

4th order, $h_S = 60°$, sunward hemisphere, left: all orders, center: only 3rd-7th order, right: dominant ray path for $a_0 = 1{,}1\ \mathrm{mm}$. Due to the dominant 0th order background, this spot will require methods as described in [65, 66] to be extracted, even in the most favorable case of zero tilts.

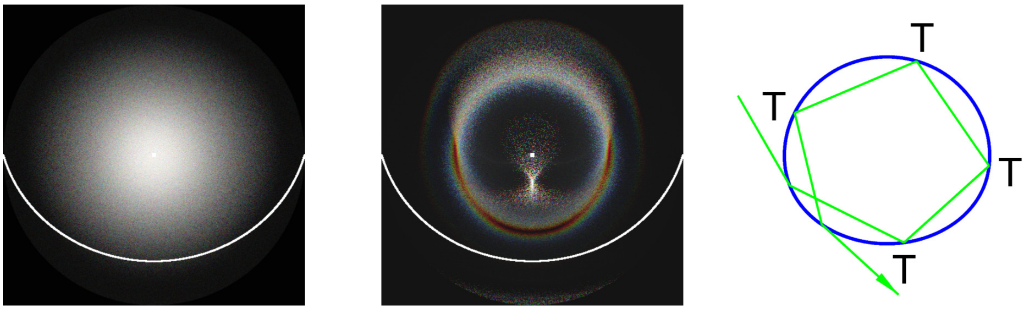

2nd order, $h_S = 6°$, antisolar hemisphere (see Fig. 3a-c for comparison)

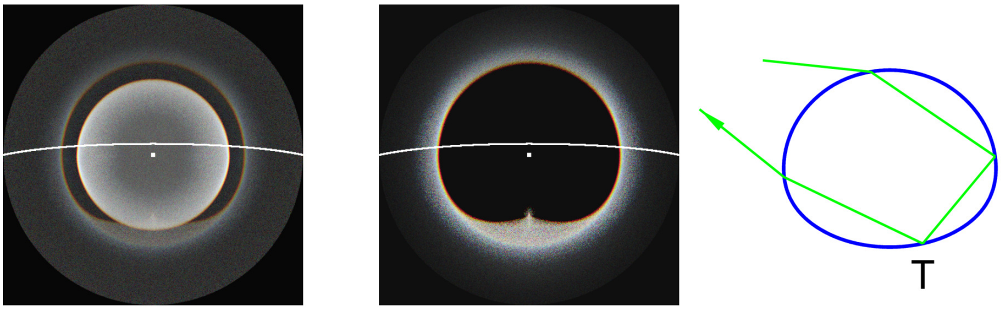

6th order, $h_S = 36°$, antisolar hemisphere (see Fig. 3g-i for comparison)

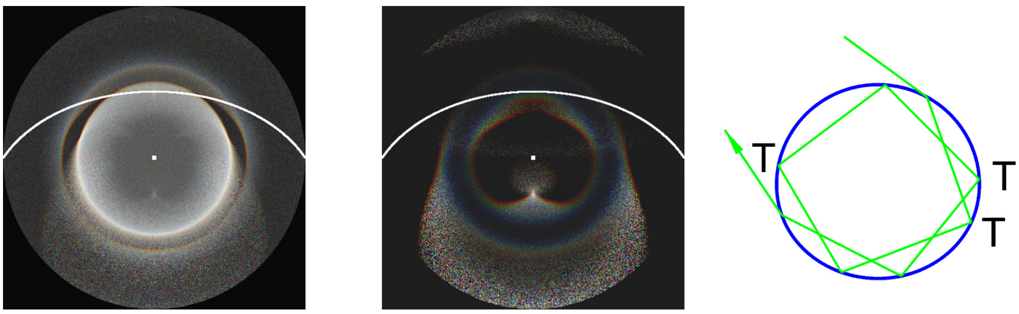

5. Caustic evolution near the critical drop size

- example: 2nd order (all other orders switched off), $h_S = 36°$, antisolar hemisphere
- same intensity scaling for all images (i.e., raw intensities divided by geometric optical cross section of the drop and mapped to RGB, followed by identical non-linear brightness processing)

$a_0 = 0.1$ mm : near-spherical reference

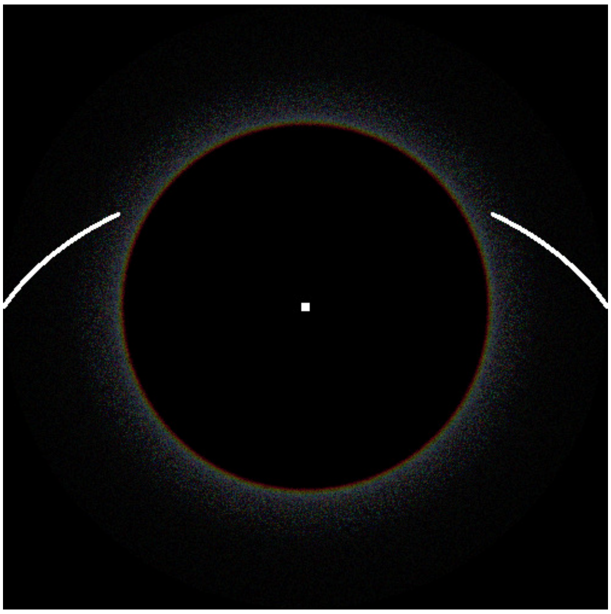

$a_0 = 1.4$ mm : upper part of caustic brighter and shifted with respect to spherical case

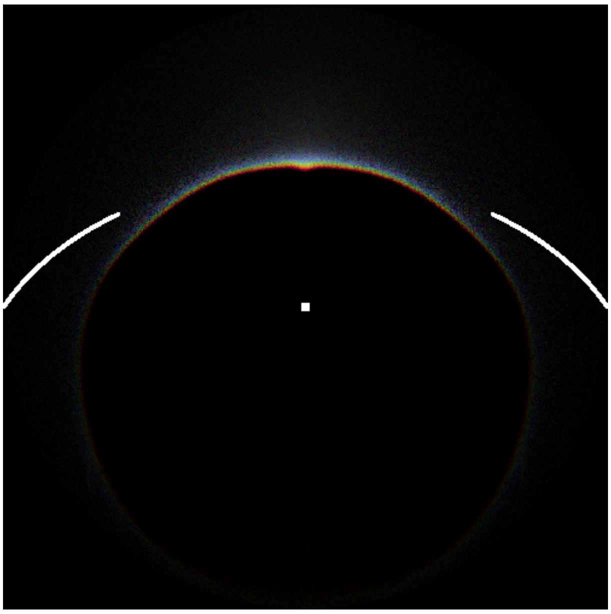

$a_0 = 1.6$ mm : ≈ critical size, cusp-like caustic above the antisolar point, intensity maximum

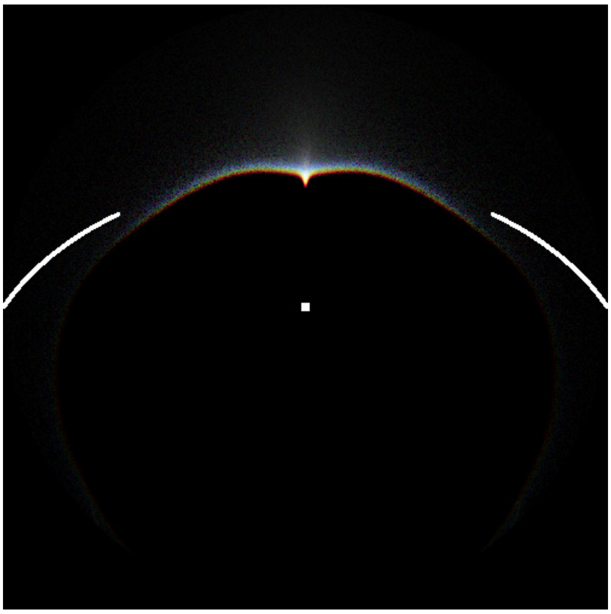

$a_0 = 1.8$ mm : involuted caustic

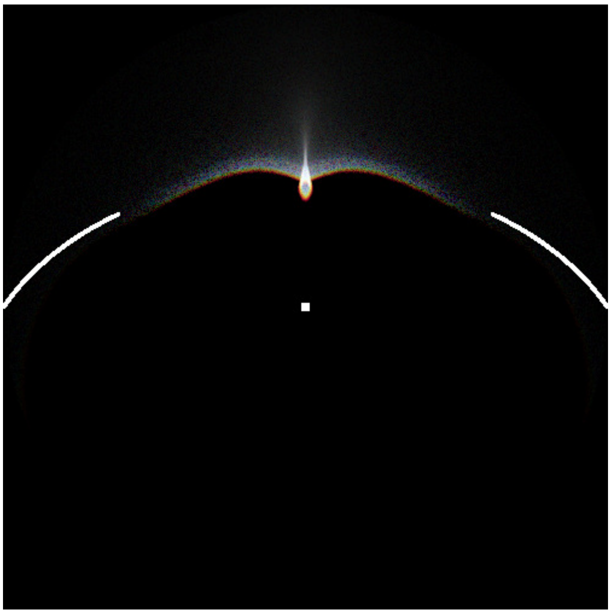

6. Animated GO simulations

- eDSD $\mu = 1$, $\Lambda = 3\ \mathrm{mm}^{-1}$
- sun elevation interval $-90° \le h_S \le +90°$, 2° increments, white line = horizon, white square = sun or antisolar point
- last 10 frames show rainbows from spherical drops for comparison (common intensity normalization for all frames)

sunward hemisphere, no oscillations, zero tilts:
http://dl.meteoros.de/haussmann/AHaussmann_rainbow_sunward_mu1lam3_osc0_tilt0.avi

antisolar hemisphere, no oscillations, zero tilts:
http://dl.meteoros.de/haussmann/AHaussmann_rainbow_antisolar_mu1lam3_osc0_tilt0.avi

sunward hemisphere, polydisperse (2,0) oscillations, amplitudes according to Eq. (9) and with Gaussian spreads ($\sigma_{rel} = 0.3$), Gaussian tilts ($\sigma = 7°$):
http://dl.meteoros.de/haussmann/AHaussmann_rainbow_sunward_mu1lam3_oscgauss_tilt.avi

antisolar hemisphere, polydisperse (2,0) oscillations, amplitudes according to Eq. (9) and with Gaussian spreads ($\sigma_{rel} = 0.3$), Gaussian tilts ($\sigma = 7°$):
http://dl.meteoros.de/haussmann/AHaussmann_rainbow_antisolar_mu1lam3_oscgauss_tilt.avi

7. Triple-split rainbow analyses

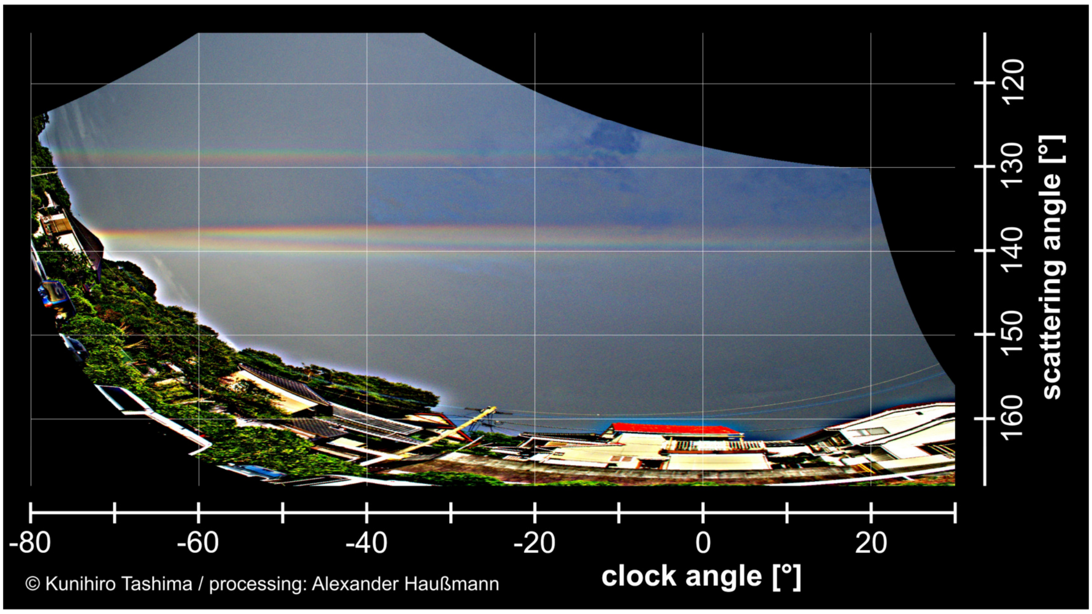

Reprojection of Fig. 5a in scattering coordinates

Triple-split rainbow photographed Aug. 12th, 2014, 17:18 CST, Yulong river, Guangxi province, China, by Liu Hai-Cheng ($h_S = 25.4°$ *)*

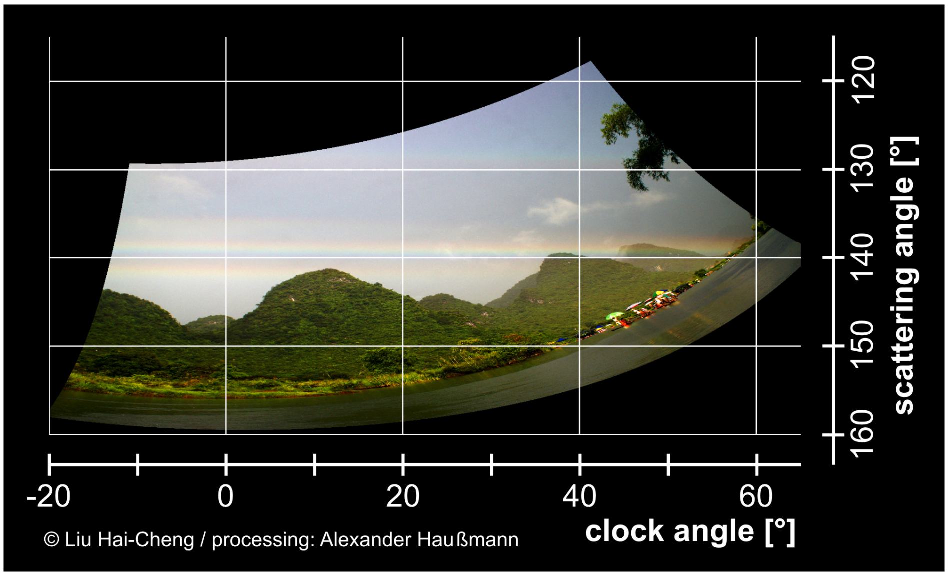

Reprojection in scattering coordinates

8. Rainbows from drops with axes tilted in a preferential orientation

- alternative explanation for non-symmetric twinning as shown in Fig. 5b, c (neglecting the weak lower branch B)
- assuming non-oscillating BC equilibrium drop shapes that can be tilted in arbitrary directions, i.e. behaving as rigid bodies
- typical eDSD for twinned rainbows (also used in [10])

$$n(a_0) = n_0 \cdot \exp(-2 \cdot a_0 \cdot \Lambda) + n_1 \cdot \exp\left(-\frac{(a_0 - \overline{a_0})^2}{2\sigma^2}\right)$$

$n_0 = 1$ (actual physical unit is not relevant), $\Lambda = 4\ \text{mm}^{-1}$, $n_1 = 0.07$, $\overline{a_0} = 0.5\ \text{mm}$, $\sigma = 0.03\ \text{mm}$

- example: no oscillations, no random tilts, but fixed tilt axis direction $\vartheta_D = 60°$, $\varphi_D = 196.4°$:

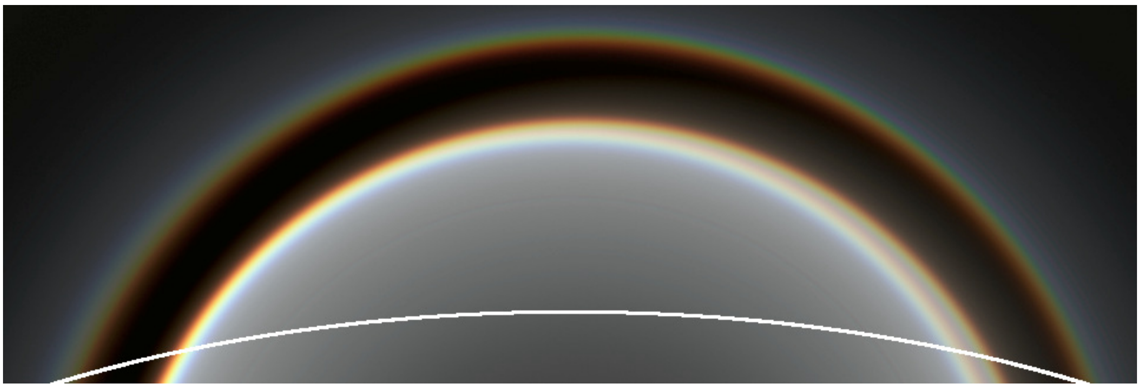

Simulation for $h_S = 25°$ *(Lambert projection centered on antisolar point, cropped), white line = horizon*

- corresponding Möbius shifts for $a_0 = 0.5$ mm , $q = 0$:

  - full range of clock angles must be displayed: in general, no left/right symmetry for tilted axes
  - same color scaling as in Sect. 3

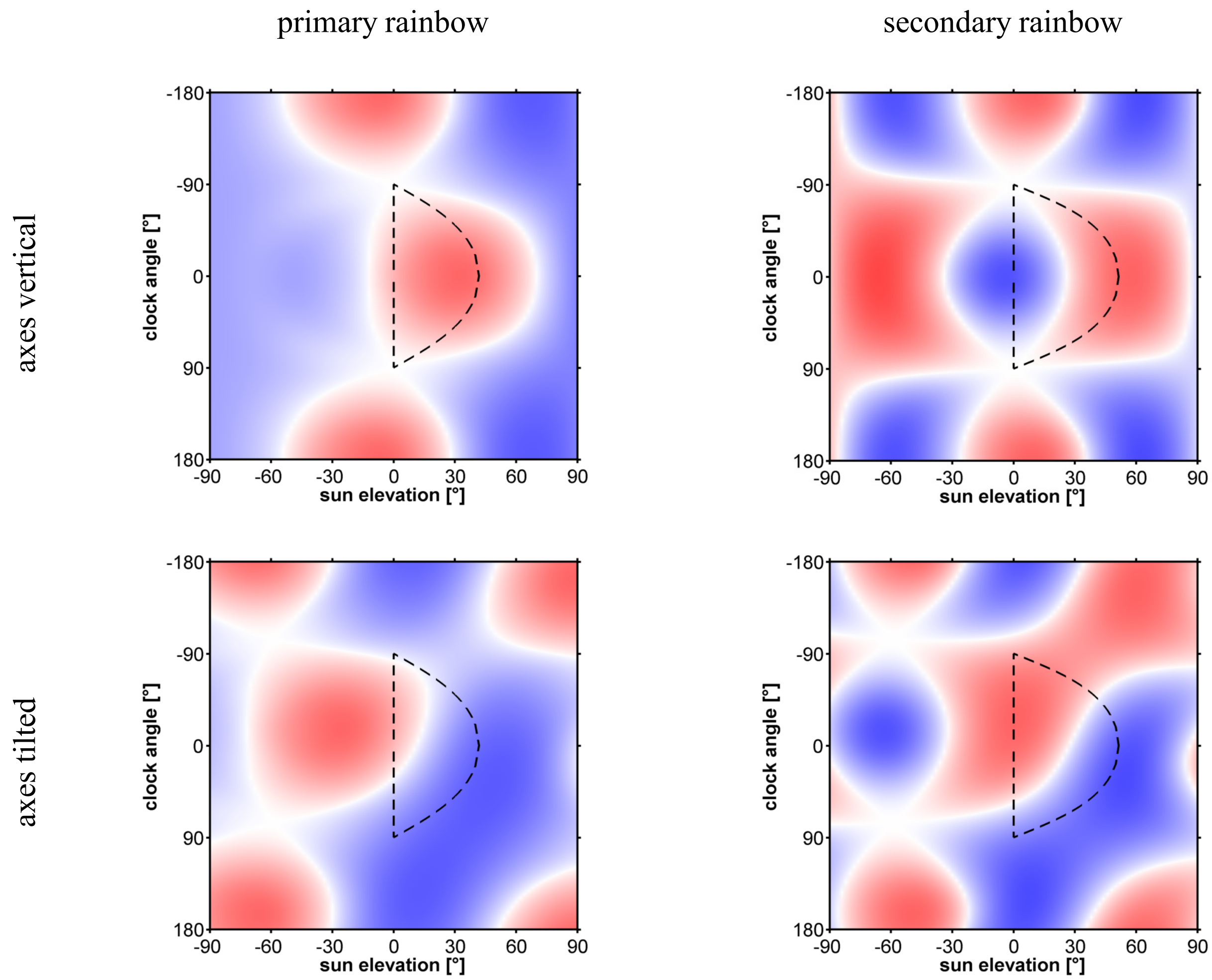

  - for vertical axes: Möbius shift for primary inside visibility segment always positive (i.e. directed towards the antisolar point)
  - properly tilted axes: negative and non-left/right-symmetric shifts occur
  - but: required tilt angles are improbably large, and even if occurring, changes of equilibrium drop shapes are to be expected (shifts have then to be recalculated)